Title

Application and reduction of a nonlinear hyperelastic wall model capturing ex vivo relationships between fluid pressure, area, and wall thickness in normal and hypertensive murine left pulmonary arteries

Authors

Haider, Mansoor A

Pearce, Katherine J

Chesler, Naomi C

et al.

Publication Date

2024-01-12

DOI

10.1002/cnm.3798

Received: Added at production | Revised: Added at production | Accepted: Added at production

DOI: xxx/xxxx

ARTICLE TYPE

Application and reduction of a nonlinear hyperelastic wall model capturing ex vivo relationships between fluid pressure, area and wall thickness in normal and hypertensive murine left pulmonary arteries †

Mansoor A. Haider*[1] | Katherine J. Pearce**[1] | Naomi C. Chesler[2] | Nicholas A. Hill[3] | Mette S. Olufsen[1]

[1]Department of Mathematics, North Carolina State University, North Carolina, USA
[2]Edwards Lifesciences Foundation Cardiovascular Innovation and Research Center & Department of Biomedical Engineering, University of California, Irvine (UCI), California, USA
[3] School of Mathematics and Statistics, University of Glasgow, Glasgow, United Kingdom

Correspondence
*Mansoor A. Haider, Department of Mathematics, North Carolina State University, Box 8205, Raleigh, NC 27695-8205 USA. Email: mahaider@ncsu.edu

Present Address
**Oden Institute for Computational Engineering and Sciences, Texas, USA

Abstract

Pulmonary hypertension is a cardiovascular disorder manifested by elevated mean arterial blood pressure (> 20 mmHg) together with vessel wall stiffening and thickening due to alterations in collagen, elastin and smooth muscle cells. Hypoxia-induced (type 3) pulmonary hypertension can be studied in animals exposed to a low oxygen environment for prolonged time periods leading to biomechanical alterations in vessel wall structure. This study introduces a novel approach to formulating a reduced order nonlinear elastic structural wall model for a large pulmonary artery. The model relating blood pressure and area is calibrated using *ex vivo* measurements of vessel diameter and wall thickness changes, under controlled pressure conditions, in left pulmonary arteries isolated from control and hypertensive mice. A two-layer, hyperelastic, anisotropic model incorporating residual stresses is formulated using the Holzapfel-Gasser-Ogden model. Complex relations predicting vessel area and wall thickness with increasing blood pressure are derived and calibrated using the data. Sensitivity analysis, parameter estimation, subset selection and physical plausibility arguments are used to systematically reduce the 16-parameter model to one in which a much smaller subset of identifiable parameters is estimated via solution of an inverse problem. Our final reduced one layer model includes a single set of three elastic moduli. Estimated ranges of these parameters demonstrate that nonlinear stiffening is dominated by elastin in the control animals and by collagen in the hypertensive animals. The pressure-area relation developed in this novel manner has potential impact on one-dimensional fluids network models of vessel wall remodeling in the presence of cardiovascular disease.

KEYWORDS:
Pulmonary hypertension; Hypoxia; Arterial wall; Model reduction; Sensitivity analysis; Identifiability; Hyperelastic pressure-area relation

1 | INTRODUCTION

Pulmonary hypertension (PH), encompassing several cardiovascular disorders manifested by a mean pulmonary arterial blood pressure (BP) above 20 mmHg, is commonly classified into five disease groups [1, 2]. One of these, group 3, "pulmonary hypertension due to lung disease", includes patients with PH induced by hypoxia (HPH). This disease type can be studied in mice with PH induced by placing animals in a low oxygen (hypoxic) environment. The response of the cardiovascular system is stiffening and thickening of the pulmonary arteries accompanied by an increase in BP to PH levels. The aim of this study is to use data-driven mathematical modeling to devise a a well-calibrated reduced model capturing the relationship between BP and changes in vessel lumen area and wall thickness that characterizes the structural remodeling of the underlying tissues. For this PH group, vascular remodeling typically starts in the small arteries, proceeding to the large arteries as the disease advances [3, 4]. The arterial wall comprises three layers, the intima, a single layer of endothelial cells, the media which contains large amounts of elastin and smooth muscle cells, and the adventitia mainly composed of collagen (Fig. 1a). In animal models of group 3 PH, vessels stiffen due to collagen accumulation [5, 6], and smooth muscle cell proliferation, which are known to increase the thickness of the vessel wall [7]. Furthermore, wall thickening in the media and adventitia are known to occur by different rates and due to different underlying mechanisms of tissue remodeling. For example, adventitial thickening typical occurs earlier and is more pronounced, with medial thickening lagging behind [8].

One advantage of characterizing how PH impacts the pressure-area relationship is that the resulting model can be incorporated into one-dimensional (1D) fluid dynamics network models used extensively to study hemodynamics in both systemic [9, 10, 11, 12, 13, 14] and pulmonary [15, 16, 17] arteries. 1D fluid dynamics models are especially well suited to predict flow distribution and wave-propagation along the network, but accurate predictions require appropriate specification of the pressure-area interaction. Moreover, 1D models can be readily calibrated to *in vivo* geometry, flow and/or BP measurements [18, 19]. The 1D fluid dynamics models are derived from the Navier-Stokes equations combined with a state equation relating blood pressure and vessel area, often formulated using an empirical or simple elastic wall model. These simpler models have the advantage of being specified using a small number of parameters [20, 13, 21, 22], but how tissue remodeling is modulated with disease is unclear. While complex tissue mechanics models exist [23, 24, 25], they have not been integrated with 1D fluid dynamics models. One state-of-the-art tissue mechanics model is the two-layer nonlinear hyperelastic model developed by Holzapfel, Gasser, and Ogden [23] (HGO model) that captures *ex vivo* biomechanical deformation of the vessel wall. While this model is complex, it includes parameters that more directly and realistically represent structural elements and constituents within the two primary tissue layers that are known to remodel in large pulmonary arteries under hypoxic conditions.

In this study, we introduce a novel data-driven approach to formulating and systematically reducing a nonlinear hyperelastic structural wall model for the large pulmonary arteries, generating a reduced pressure-area relation that can characterize remodeling in HPH. The model is calibrated to *ex vivo* biomechanical deformation and wall thickness measurements from control and hypertensive mice. Our approach to effective calibration and reduction is to start with a model having structural features that are physiologically motivated. We then fix some parameters based on procedures in the experiments and literature values appropriate to the vessel and species in our data. Using subset selection, based on local sensitivities, we systematically fix or eliminate additional model parameters that are practically unidentifiable, without violating physical plausibility of the reduced model.

To this end, we first formulate a two-layer, anisotropic vessel wall model using the HGO model formulation [23], which disregards the intima. In addition to anisotropy and multiple layers, this model accounts for residual stresses, known to be significant in large pulmonary arteries as evidenced by a large opening angle arising when rings from excised vessels are cut. The rings are obtained from cutting "a slice" normal to the axial direction, and the opening angle is determined from a radial cut through the ring's circumference [26, 27]. Complex relations determining the dependence of vessel area and wall thickness on blood pressure (BP) are derived. Our initial model is calibrated to *ex vivo* measurements of vessel diameter and wall thickness as functions of pressure in the left pulmonary artery (LPA) in control (CTL) and hypertensive (HPH) mice [28]. The full model is complex, containing 16 parameters, making calibration and model reduction using data challenging. Our approach to effective model calibration and reduction combines sensitivity analysis, subset selection [29, 30, 31, 32] and physical plausibility arguments to identify the simplest reduced model and a set of sensitive and identifiable parameters that can be estimated using the model and available data.

[†]Supported in part by the US National Science Foundation (DMS-1615820, DMS-1638521) and by U.K. Research and Innovation (EPSRC EP/N014642/1, EP/S030875/1, EP/T017899/1), and a Leverhulme Research Fellowship (NAH). The authors would also like to acknowledge Michelle Bartolo for developing the digital illustration in Fig. 1a.

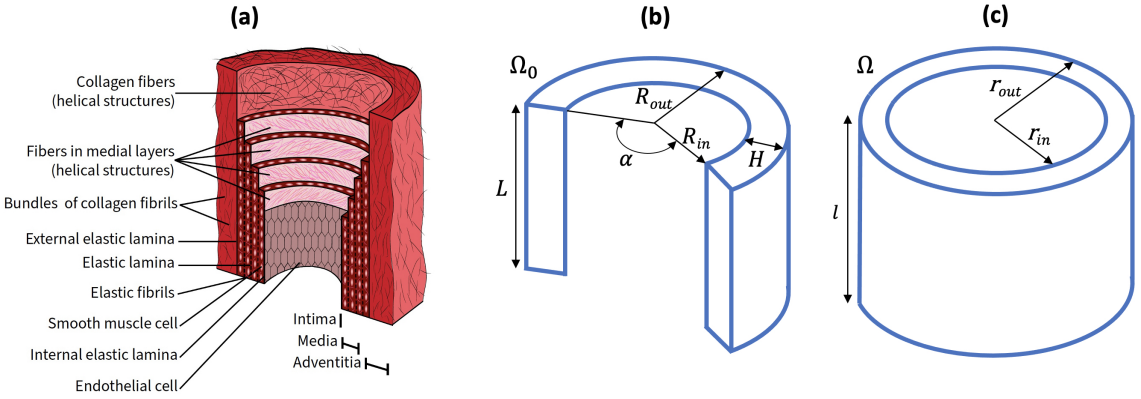

Figure 1 Foundations of the nonlinear hyperelastic wall model: (a) Illustration of a cross-section of a large artery wall (redrawn from [23]); (b) the stress-free reference state Ω_0 defined in equation (1) where R_{in} is the inner radius, R_{out} is the outer radius, H is the wall thickness, L is the axial length and α is the opening angle; (c) the current configuration Ω defined in (2). Note that the (deformed) inner radius (r_{in}), outer radius (r_{out}) and axial length (l) are all determined after the model equations are solved.

2 | MODELS AND METHODS

1D cardiovascular fluid dynamics network models require a constitutive relation coupling the transmural blood pressure $p(z,t)$ (mmHg) (the difference between blood pressure in the vessel and the surrounding tissue) to the vessel lumen area $a(z,t)$ (cm^2). We represent the vessel wall as a hyperelastic material integrating the two layer model by Holzapfel, Gasser and Ogden, often referred to as the HGO model [23]. This model incorporates nonlinear effects of residual stresses, anisotropy, material and geometric nonlinearities, and contributions of key wall constituents (collagen and elastin) within the vessel wall layers. A schematic of the wall constituents is shown in Fig. 1, and Table 4 (in the Appendix) lists the model parameters and their units.

2.1 | Deformation of the arterial wall

The model is formulated in terms of three configurations of the vessel wall: (i) a *stress-free* reference state Ω_0 (Fig. 1b) represented by a continuous arc of a cylindrical ring free of all residual stresses; (ii) an intermediate *load-free* configuration (not shown) represented by a closed cylindrical ring in the absence of transmural pressure; and (iii) a *current* configuration Ω (Fig. 1c) representing the pressurized vessel under an isochoric deformation as fluid flows through the vessel lumen in an *ex vivo* or *in vivo* setting.

Stress-free reference state: Ω_0 approximates the process of excising a vessel segment, extracting a cross-section approximated as a thin cylindrical ring, and then making a single radial cut along the ring's circumference. It is denoted by

$$\Omega_0 = \left\{ \left(R, \Theta, Z\right) \in [R_{in}, R_{out}] \times [0, 2\pi - \alpha] \times [0, L] \right\}, \tag{1}$$

where $\left(R, \Theta, Z\right)$ are Lagrangian cylindrical (polar) coordinates, α is the opening angle, L is the reference axial length, and R_{in} and R_{out} are the inner and outer radii, respectively.

Current configuration: Ω (shown in Fig. 1c) is associated with the deformed vessel representing the coupled state under fluid flow and pressure and defined as

$$\Omega = \left\{ \left(r, \theta, z\right) \in [r_{in}, r_{out}] \times [0, 2\pi] \times [0, l] \right\}, \tag{2}$$

where the deformation determines the (unknown) inner radius (r_{in}), the outer radius (r_{out}), and the vessel length (l).

Finally, an isochoric deformation arising from combining inflation, axial extension, and torsion within an elastic tube is denoted by

$$\left(r, \theta, z\right) = \left(\sqrt{\frac{R^2 - R_{in}^2}{k\lambda_z} + r_{in}^2}, k\Theta + Z\frac{\Phi}{L}, \lambda_z Z \right), \tag{3}$$

where $k = \frac{2\pi}{2\pi - \alpha}$, λ_z is the (constant) axial stretch and Φ is the twist angle. As reported in [28], for the data used in this study $\lambda_z = 1.4$ for both the control and hypertensive animals, corresponding to the observed ratio of the axial length of a vessel

segment before and after excision. We note that $\lambda_z > 1$ due to residual stresses *in vivo*. The *ex vivo* measurements of deformation, after introducing fluid flow through the vessel, are performed in vessels stretched and mounted to match this measured ratio.

2.2 | Two-layer hyperelastic model

Within the HGO framework, a two-layer hyperelastic wall model accounting for the media ($\gamma = M$) and adventitia ($\gamma = A$) (Fig. 1a) is formulated by representing the Cauchy stress $\sigma = \sigma_M + \sigma_A$ as the sum of the stress in each layer [23],

$$\sigma_\gamma = c_\gamma \text{dev}\left(J^{-\frac{2}{3}}\mathbf{b}\right) + 2\frac{\partial \Psi_\gamma}{\partial \tilde{I}_{4\gamma}}\text{dev}\left(\mathbf{a}_{1\gamma}\otimes\mathbf{a}_{1\gamma}\right) + 2\frac{\partial \Psi_\gamma}{\partial \tilde{I}_{6\gamma}}\text{dev}\left(\mathbf{a}_{2\gamma}\otimes\mathbf{a}_{2\gamma}\right), \quad \gamma = M, A, \tag{4}$$

where Ψ_γ, the Helmholtz free energy for each layer, has the form

$$\Psi_\gamma = \frac{k_{1\gamma}}{2k_{2\gamma}}\left[e^{k_{2\gamma}\left(\tilde{I}_{4\gamma}-1\right)^2} + e^{k_{2\gamma}\left(\tilde{I}_{6\gamma}-1\right)^2} - 2\right], \quad \gamma = M, A. \tag{5}$$

In equation (4), c_γ represent the elastic moduli for the isotropic constituents (mostly elastin) in each layer, $J = \det\left(\mathbf{F}\right)$, is the Jacobian where $\mathbf{F}$ is the deformation gradient of (3), $\mathbf{b} = \mathbf{F}\mathbf{F}^T$, and $\tilde{I}_{l\gamma} = \mathbf{A}_{l\gamma} : \bar{\mathbf{C}}$ where $\bar{\mathbf{C}} = J^{-2\hbar 3}\mathbf{C}$, $\mathbf{C} = \mathbf{F}^T\mathbf{F}$ and $\mathbf{A}_{l\gamma} = \mathbf{a}_{0l\gamma}\otimes\mathbf{a}_{0l\gamma}$ $\left(l = 4, 6,\ \gamma = A, M\right)$. In (5), $k_{1\gamma}$ and $k_{2\gamma}$ are elastic parameters for the anisotropic constituents (mostly collagen) in each layer (Fig. 1a). Lastly, Eulerian and Lagrangian vectors, $\mathbf{a}_{l\gamma}$ and $\mathbf{a}_{0l\gamma}$ (respectively), associated with collagen fiber directions are ($\gamma = A, M$)

$$\mathbf{a}_{l\gamma} = J^{-\frac{1}{3}}\mathbf{F}\mathbf{a}_{0l\gamma},\ \mathbf{a}_{0l\gamma} = \begin{pmatrix} 0 \\ \cos\left(\beta_\gamma\right) \\ \pm\sin\left(\beta_\gamma\right) \end{pmatrix}, l = 4, 6, \tag{6}$$

where β_γ are the collagen fiber angles, assumed to be constant in each layer (Fig. 1a).

2.3 | Pressure-area relation

We obtain a hyperelastic pressure-area relation by integrating the radial component of the stress equilibrium equation. Neglecting inertial terms and assuming a quasi-static state this stress equilibrium equation, expressed in the current configuration, is given by

$$\frac{d\sigma_{rr}}{dr} + \frac{\sigma_{rr} - \sigma_{\theta\theta}}{r} = 0, \quad r_{in} < r < r_{out}, \tag{7}$$

where $r_{in} = r\left(R_{in}\right)$ and $r_{out} = r\left(R_{in} + H\right)$, and $\sigma_{rr}, \sigma_{\theta\theta}$ are the radial and circumferential normal stress components, respectively. Here, H denotes the undeformed vessel wall thickness (Fig. 1b).

Balance of forces between the transmural blood pressure and the radial component of the normal stress in the wall is enforced by the condition,

$$p = -\sigma_{rr}\big|_{r=r_{in}} \Rightarrow p = \int_{r_{in}}^{r_{out}} \frac{\sigma_{rr} - \sigma_{\theta\theta}}{r}\,dr. \tag{8}$$

Equations (3-4) are used to formulate the integrand in (8), which is evaluated with the aid of symbolic computation software (MAPLE 2019).

The resulting pressure-area relation can be written as

$$p = \int_{r_{in}}^{r_{MA}} \mathcal{F}_M\left(r_{in}, r\right) dr + \int_{r_{MA}}^{r_{out}} \mathcal{F}_A\left(r_{in}, r\right) dr, \quad \text{where } r_{MA} = r\left(R_{in} + H_M\right), \tag{9}$$

and H_M is the (reference) thickness of the media. Recall that the relation $r_{in} = \sqrt{\frac{a}{\pi}}$ is used to express the inner radius (9) in terms of the vessel area. For brevity, the mathematical forms of the integrands $\mathcal{F}_M$ and $\mathcal{F}_A$ are not included here as these are lengthy expressions imported from MAPLE into MATLAB (R2021b). The integral is evaluated numerically using the MATLAB "integral" command which employs global adaptive quadrature [33].[1]

[1]The code for this evaluation will be publicly available via a github link at http://haider.wordpress.ncsu.edu as of Nov. 15, 2022.

This final pressure-area relation (9) contains 16 model parameters

$$\mathbf{q} = [R_{in}, R_{out}, H, H_M, \alpha, L, \Phi, \lambda_z, c_M, k_{1M}, k_{2M}, \beta_M, c_A, k_{1A}, k_{2A}, \beta_A], \tag{10}$$

listed with units and values in the Appendix (Table 4). For any given set of values of these parameters, the model prediction of wall thickness is evaluated using equations (9) and (3) via the difference $r\left(R_{in}+H\right)-r\left(R_{in}\right)$.

2.4 | Ex vivo murine data

The model is calibrated to murine data made available by Naomi Chesler (UC Irvine). The majority of the data along with detailed descriptions of the experiments can be found in the study by Tabima and Chesler [28]. All protocols and procedures described in [28] were approved by the University of Wisconsin Institutional Animal Care and Use Committee.

Data measuring lumen area and wall thickness changes with increasing transmural blood pressure were measured under *ex vivo* biomechanical testing in excised left pulmonary artery (LPA) vessel segments from male C57BL6 mice under control (CTL) and 10-day hypoxia-induced (380 mmHg) hypertensive (HPH) conditions [28]. In both the control (CTL) and hypertensive (HPH) vessel segments, 11 measurements ($i = 1, \dots, 11$) relate vessel outer diameter (D_i^{data}) to increasing pressure (p_i^{data}), and 3 measurements ($j = 1, 2, 3$) relate vessel wall thickness (T_j^{data}) to increasing pressure (p_j^{data}). For each group, these measurements represent averages over 4 control (CTL) and 5 hypertensive (HPH) animals under controlled pressure conditions with pressures in the range of 0-50 mmHg. Specific pressure values for each group are noted in Fig. 2a-b.

2.5 | Model parameters

Several of our model parameters are fixed at representative values using literature values or details of the experiments used to calibrate the models. First, we assume that the vessels have no twist, i.e. $\Phi = 0°$ and that the opening angle in the stress-free reference state is $\alpha = 94.2°$. The latter value is obtained from literature reporting measurements in rings extracted from healthy murine LPA vessels [27]. To mimic the *in vivo* setting, excised vessels were stretched to match their length after extraction prior to mechanical testing [28], i.e., $\lambda_z = 1.4$ in (3).

Control animal parameters. Since detailed histology for the murine LPA is not available, we use a recent literature value estimating a mean diagonal collagen fiber angle of 35.55° (measured from the axial direction) in the right pulmonary artery (RPA) of normoxic mice [34], corresponding to a value of $\beta_M = \beta_A = 54.45°$ in our control animal model (CTL). In addition, from the same study [34], we assume that the media occupies 63% of the vessel wall thickness in the stress-free reference state for our control model.

Hypertensive animal parameters. For our hypertensive model, two cases are considered. In the first case (HPH^a), the fiber angle and media thickness percentage values are the same as in the CTL case. In the second case (HPH^b), the fiber angle values are fixed at $\beta_M = \beta_A = 56.58°$ and the media thickness percentage is fixed at 60%. Because our data set is based on 10-days of hypoxic exposure, these values are calculated as a 30% perturbation in the direction of the hypertensive values reported in [34], where murine RPA was exposed to to 3-6 weeks of hypoxic conditions; the values in [34] are a mean diagonal fiber angle of 28.45° (measured from the axial direction) and a media thickness percentage of 53%. For both hypertensive cases that we consider, the opening angle value ($\alpha = 94.2°$ [27]) is chosen to be the same as in the control model, based on the only known measurements of this quantity in a similar vessel and species after 10-days of hypoxic conditions [26] (see Fig. 7 therein). The fixed parameter values are summarized in the Appendix (Table 4).

Accounting for these assumptions, for the parameter dependency $R_{out} = R_{in} + H$, and observing that the model is independent of L yields the following 8 parameters to be estimated

$$\mathbf{q}_8 = [R_{in}, H, c_M, k_{1M}, k_{2M}, c_A, k_{1A}, k_{2A}]. \tag{11}$$

2.6 | Parameter estimation, sensitivity, identifiability and model reduction

Given the model and data, we formulate a parameter estimation problem determining m parameters $\mathbf{q}^*$ minimizing the least squares cost $\mathcal{J}$ as

$$\mathbf{q}^* = \arg\min_{\mathbf{q}\in\mathbb{R}^m_{\geq 0}} \mathcal{J}\left(\mathbf{q}\right), \quad \text{where: } \mathcal{J}\left(\mathbf{q}\right) = \mathbf{s}\left(\mathbf{q}\right)^T \mathbf{s}\left(\mathbf{q}\right). \tag{12}$$

The 14-component residual vector $\mathbf{s}\left(\mathbf{q}\right)$ is given by

$$\begin{aligned} \mathbf{s}\left(\mathbf{q}\right) &= \left[\mathbf{s}_1, \mathbf{s}_2\right], \\ \mathbf{s}_1 &= \frac{1}{\sqrt{n_1}}\left(\frac{p\left(a_{\text{in},i}\right) - p_i^{\text{data}}}{p^*}\right), \\ \mathbf{s}_2 &= \frac{1}{\sqrt{n_2}}\left(\frac{T\left(p_j^{\text{data}}\right) - T_j^{\text{data}}}{T_1^{\text{data}}}\right), \end{aligned} \tag{13}$$

with $i = 1, \ldots, n_1$ and $j = 1, \ldots, n_2$, with $n_1 = 11$ and $n_2 = 3$ (see §2.4). The optimization problem is solved using a Nelder-Mead direct search simplex algorithm [35] minimizing $\mathcal{J}\left(\mathbf{q}\right)$ in (12) using the routine "fminsearch" in Matlab.

The mathematical model is used to evaluate the term $a_{\text{in},i}$ by first converting the outer diameter data (D_i^{data}) to an inner radius using equation (3) and then using equation (9) to determine the values $p\left(a_{\text{in},i}\right)$. The term $T\left(p_j^{data}\right)$ is evaluated as outlined at the end of §2.3. Calibration of the model to data is done in an iterative manner, gradually reducing the model complexity and number of parameters estimated using sensitivity analysis and subset selection.

Sensitivity analysis is performed after parameter estimation (with n data points) using local methods calculating the $n \times m$ sensitivity matrix $\chi = \nabla_{\mathbf{q}}\mathbf{s}\left(\mathbf{q}\right)$ using a first-order finite-difference scheme. Prior to calculation of sensitivity derivatives, a linear mapping is used to normalize across scales. Specifically, a perturbed interval (perturbation α) about the kth component of the parameter estimate $[\left(1-\alpha\right)q_k^*, \left(1+\alpha\right)q_k^*]$ is mapped to $[0, 1]$ via the linear transformation $y = \frac{1}{2\alpha}\left(\alpha - 1 + \frac{x}{q_k^*}\right)$. This yields, via the Chain rule, the derivative transformation $\frac{\partial}{\partial x} = \frac{dy}{dx}\frac{\partial}{\partial y}$, resulting in a multiplying factor $2\alpha q_k^*$ used for transforming raw sensitivities to their scaled counterparts. A value $\alpha = 0.1$ is prescribed and all sensitivity derivatives above are approximated using first-order finite-difference approximations with a step size chosen sufficiently small (10^{-7}). This choice ensures numerical convergence of all scaled parameter sensitivity derivative computations across all cases considered in this study.

Subset selection and model reduction is performed using the eigenvalue method [29, 30, 31, 32] that analyzes the magnitude of eigenvalues and corresponding eigenvectors for the $m \times m$ Fisher information matrix approximated as $\chi^T\chi$ at $\mathbf{q} = \mathbf{q}^*$ [36]. In our study, the eigenvalue subset selection method is also guided by physical plausibility of our model at each stage of the overall process. At $\mathbf{q} = \mathbf{q}^*$, the subset selection analysis and model reduction uses the following iterative procedure:

1. Determine the eigenvalues of the Fisher information matrix $\chi^T\chi$.
2. Check if the smallest eigenvalue of $\chi^T\chi$ is below a specified threshold η (see, e.g. Fig. 4).
3. If step 2 is satisfied, examine the eigenvector corresponding to the smallest eigenvalue.
4. Mark the order 1 components of the eigenvector in step 3.
5. Parameters corresponding to the marked vector components in step 4 are potentially *unidentifiable* and considered as candidates for fixing at nominal values, or uncovering parameter dependencies.
6. If possible, we reduce the model by fixing or eliminating unidentifiable parameters.

During the course of this iterative procedure, we ensure that the cost $\mathcal{J}\left(\mathbf{q}^*\right)$ is preserved. This approach strikes a balance between model reduction and robust optimization, preserving the quality of curve-fits within the context of the given data set as the process advances. We defer parameter estimation for the HPH animals until identifiability analysis and model reduction are carried out for the CTL animals. This approach ensures that the healthy and diseased cases are compared by solving a more robust inverse problem on an equal footing, i.e. with the same set of unidentifiable parameters fixed or eliminated.

3 | RESULTS

We apply the following iterative approach for estimating the non-fixed parameters in (11):

§3.1 Estimate the 8 non-fixed parameters for the control animals. Results of parameter estimation, sensitivity analysis, and subset selection yield a reduced model with 6 parameters.

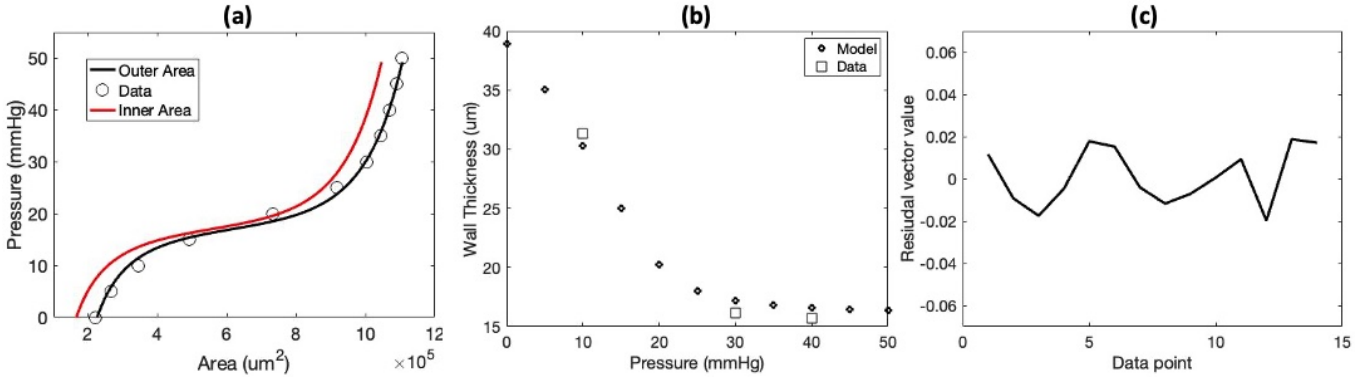

Figure 2 Results from estimating 8 parameters (listed in Table 1) for the control (CTL) animals. (a) pressure vs. area, model predictions of the outer area (black) vs. data (circles) and the inner area (red); (b) wall thickness vs. pressure model predictions compared to the 3 data points (squares); (c) the residual vector (13) across the 14 data points.

§3.2 Estimate these 6 parameters for the control animals using the reduced model. Results of this analysis enable further model reduction, yielding a reduced-order model with equal elastic moduli in the two layers. The resulting model has 5 parameters.

§3.3 Estimate these 5 parameters in the reduced-order model for both control and hypertensive animals. Results indicate that the remaining parameters may be correlated. Fixing one of the correlated parameters yields the final 4-parameter reduced-order model.

§3.4 Examine parameter dependencies in a 4-parameter reduced-order model. To investigate effects of fixing one of the correlated parameters identified in §3.3, we evaluate impacts of varying the fixed parameter. We report parameter ranges for successful results, i.e., those preserving physical plausibility and quality of curve-fits via bounds on the least squares error for both control and hypertensive animals.

3.1 | Baseline control animal model (8 parameters)

We first estimate the 8 non-fixed parameters for the control animals

$$\mathbf{q}_8 = [R_{in}, H, c_M, k_{1M}, k_{2M}, c_A, k_{1A}, k_{2A}]. \tag{14}$$

Initial and estimated parameter values for this case are reported in Table 1 (initial values are also given in Table 4 (Appendix)).

The initial value of R_{in} (1 mm) is set using an order of magnitude estimate for the LPA. The initial value for the reference wall thickness H, which is highly sensitive to the wall thickness data, is set by systematically multiplying the data measurement at 10 mmHg in the experiments (see Fig. 2b) by a factor between 1 and 1.5, in increments of 0.05 (11 values). Setting initial values for the remaining 6 parameters is challenging given that experiments do not measure these parameters, but outcomes of the model (the wall thickness and the pressure-area dynamics). These parameters have physical interpretations, but they represent quantities that cannot be directly measured experimentally. The isotropic elastic moduli c_M, c_A are set to initial values of 10 kPa, an accurate order of magnitude estimate for this type of biological soft tissue. Initial values for the remaining parameters are determined by systematic variation of initial parameter choices, rejecting combinations yielding a high cost $\mathcal{J}$. This results in a set of initial values with a curve fit to the data of good quality. The combination of initial values for k_{1M} and k_{1A} is 1 kPa and 0.3 kPa, respectively and the initial values for the (dimensionless) parameters k_{2M} and k_{2A} are based on those reported in the HGO study [23] from measurements in rabbit carotid arteries. This combination of initial values yields the most consistent set of results across all cases considered.

Model predictions with estimated parameters depicting pressure vs. area and the wall thickness vs. pressure (shown in Fig. 2a and b) provide excellent fits to the control animal data. Inspection of estimated parameters reveals that the adventitia parameter k_{1A} is very small ($k_{1A} << c_A$, Table 1). This finding implies that we can eliminate the anisotropic terms for the adventitia

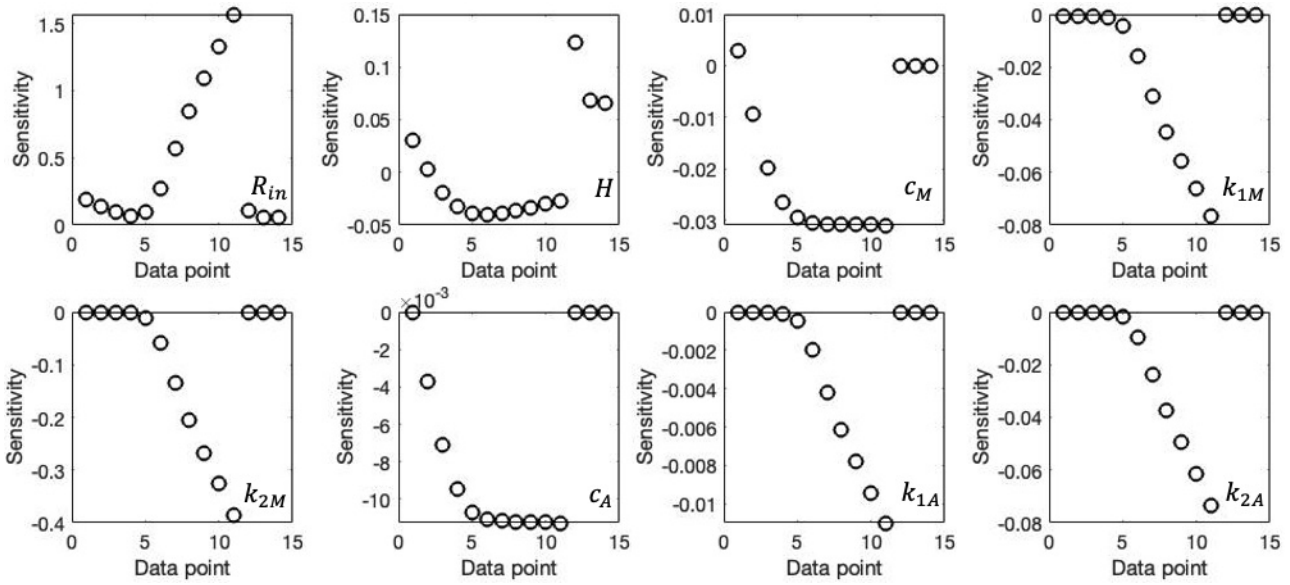

Figure 3 Normalized parameter sensitivities for the control (CTL) animals with 8 estimated parameters across the 14 data points.

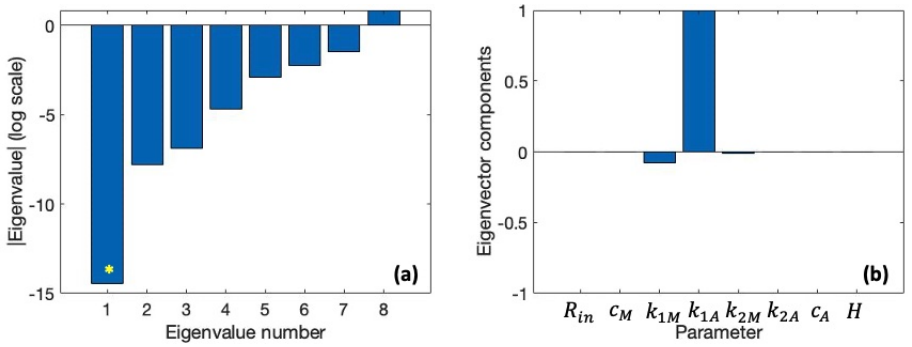

Figure 4 Identifiability results using the eigendecomposition of the information matrix ($\chi^T\chi$) for the control (CTL) animals with 8 estimated parameters: (a) log-plot of the eigenvalues of $\chi^T\chi$; (b) components of the eigenvector of $\chi^T\chi$ corresponding to the smallest eigenvalue of $\chi^T\chi$ ($\eta \approx 10^{-14}$) (asterisk).

(the last two terms in equation (4)) since their mechanical contribution to the response is insignificant. In particular, when k_{1A} is set to zero, the adventitia parameter k_{2A} is structurally unidentifiable since it can be varied arbitrarily when equation (5) is substituted into equation (4).

The Fisher information matrix $\chi^T\chi$ is used to evaluate the eigenvalues depicted in Fig. 4a. Examination of the eigenvector of $\chi^T\chi$ (Fig. 4c) corresponding to its smallest eigenvalue ($\eta \approx 10^{-14}$) flags the parameter k_{1A} (has an order 1 component), indicating that this parameter is unidentifiable. This designation is consistent with results of sensitivity analysis (shown in Fig. 3), which demonstrate that the sensitivities for k_{1A} (and c_A) are small relative to the other parameters.

Taken together, these findings suggest a physically motivated model reduction in which $k_{1A} = k_{2A} = 0$. Thus, in the next step we analyze a 6-parameter reduced model eliminating the anisotropic terms for the adventitia in the stress-strain law.

3.2 | Reduced control animal model (6 parameters)

Parameter values are initialized as described in §3.1. The 6 parameters to be estimated for the control animals are

$$\mathbf{q}_6 = [R_{in}, H, c_M, k_{1M}, k_{2M}, c_A]. \tag{15}$$

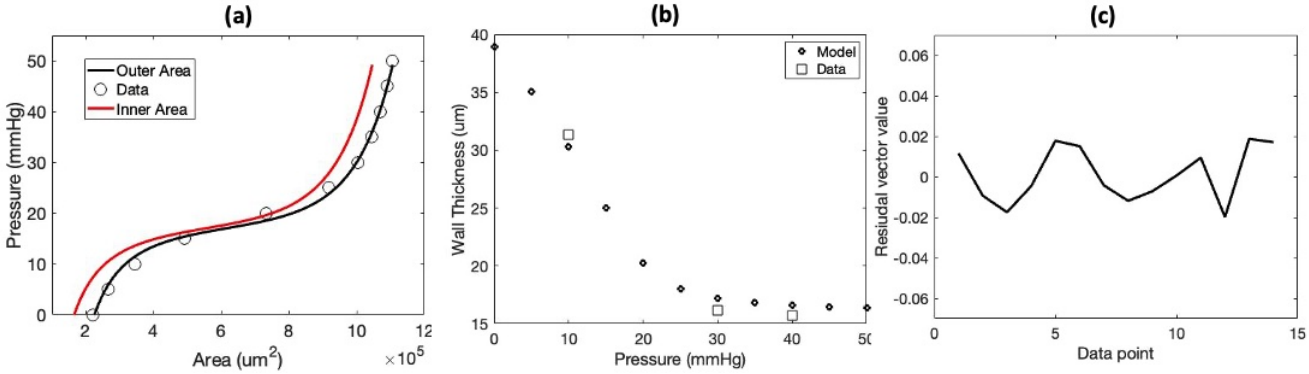

Figure 5 Parameter estimation results for the reduced model for the control (CTL) animals with 6 estimated parameters: (a) pressure vs. area model predictions of the outer area (black) vs. data (circles) and the inner area (red); (b) wall thickness vs. pressure model predictions compared to the 3 data points (squares); (c) plot of the residual vector (13) across the 14 data points.

Estimated values for these parameters are reported in Table 1. Again, for the control animals the quality of curve fits of the model to the pressure vs. area data (Fig. 5a) and the wall thickness vs. pressure data (Fig. 5b) is preserved. A very slight increase in the overall cost from $\mathcal{J} = 1.731 \cdot 10^{-4}$ to $\mathcal{J} = 1.732 \cdot 10^{-4}$ is observed. The estimated values of the geometric parameters (R_{in}, H) are preserved within 0.02%. The elastic modulus c_M exhibits a 0.9% increase, the elastic modulus k_{1M} exhibits a 10.3% increase while the elastic modulus c_A exhibits a 2.9% reduction. Finally, the dimensionless parameter k_{2M} increases by 0.9%.

Examination of the eigenvector of $\chi^T \chi$ (Fig. 6h) corresponding to its smallest eigenvalue ($\eta \approx 10^{-7}$) shown in Fig. 6g flags two parameters c_A and c_M with order 1 components; c_A is the dominant parameter. The sensitivity for c_A is also small relative to the other parameters (Fig. 6a-f). While the overall identifiability of estimated parameters in our model improves (Fig. 4a vs. Fig. 6g), these findings motivate a further reduced 5-parameter model examined in the next stage of the process.

Since two of the remaining 5 parameters are geometric parameters, we retain three elastic parameters describing the isotropic and anisotropic responses in the model in terms of a single (combined) layer. The reduced-order model analyzed in the next section has elastic moduli and collagen fiber orientation angles in the media and adventitia that are set equal. Thus, only a single set of elastic parameters are estimated in the next step. For convenience, these three estimated parameters are denoted by c_M, k_{1M} and k_{2M}.

3.3 | Reduced-order control and hypertensive animal model (5 parameters)

In the reduced-order 5-parameter model, elastic parameters in the two layers are assumed equal, i.e., $c_A = c_M$, $k_{1A} = k_{1M}$, and $k_{2A} = k_{2M}$. The parameter vector estimated for this model is

$$\mathbf{q}_5 = [R_{in}, H, c_M, k_{1M}, k_{2M}]. \tag{16}$$

This model is fitted to data from both the control (CTL) and hypertensive (HPH) animals. Values of the five model parameters are initialized as described in §3.1 and the estimated parameter values are reported in Table 2. For comparison, results of the 6-parameter model are also included in the table. Note that the estimated values of c_M, k_{1M}, and k_{2M} should be interpreted as aggregate elastic parameters for the entire vessel wall, i.e., representing both layers.

For the control (CTL) animals, the quality of curve fits of the model to the pressure vs. area data (Fig. 7a) and the wall thickness vs. pressure data (Fig. 7b) are preserved, with a reduction in overall cost from $\mathcal{J} = 1.732 \cdot 10^{-4}$ to $\mathcal{J} = 1.693 \cdot 10^{-4}$. All 11 initial values of the wall thickness parameter (H) result in identical parameter estimates, indicating increased robustness of the optimization subsequent to model reduction via identifiability analysis. The curve fits for both hypertensive models have significantly lower costs ($\mathcal{J} = 0.5297 \cdot 10^{-4}$ & $\mathcal{J} = 0.5298 \cdot 10^{-4}$) due, in part, to the smaller range of variation in the pressure-area curve caused by vessel wall stiffening (Fig. 7a & Table 2). In the hypertensive animals, geometric parameters exhibit an increase in vessel wall inner radius R_{in} (514μm & 498μm vs. 377μm) and an (expected) increase in reference wall thickness H (49μm & 50μm vs. 45μm). The altered dynamics in the hypertensive animals are reflected by a substantial increase in the elastic modulus k_{1M} (3.06kPa & 1.90kPa vs. 0.18kPa) and in the dimensionless parameter k_{2M} (7.08 & 7.12 vs. 2.19), both associated

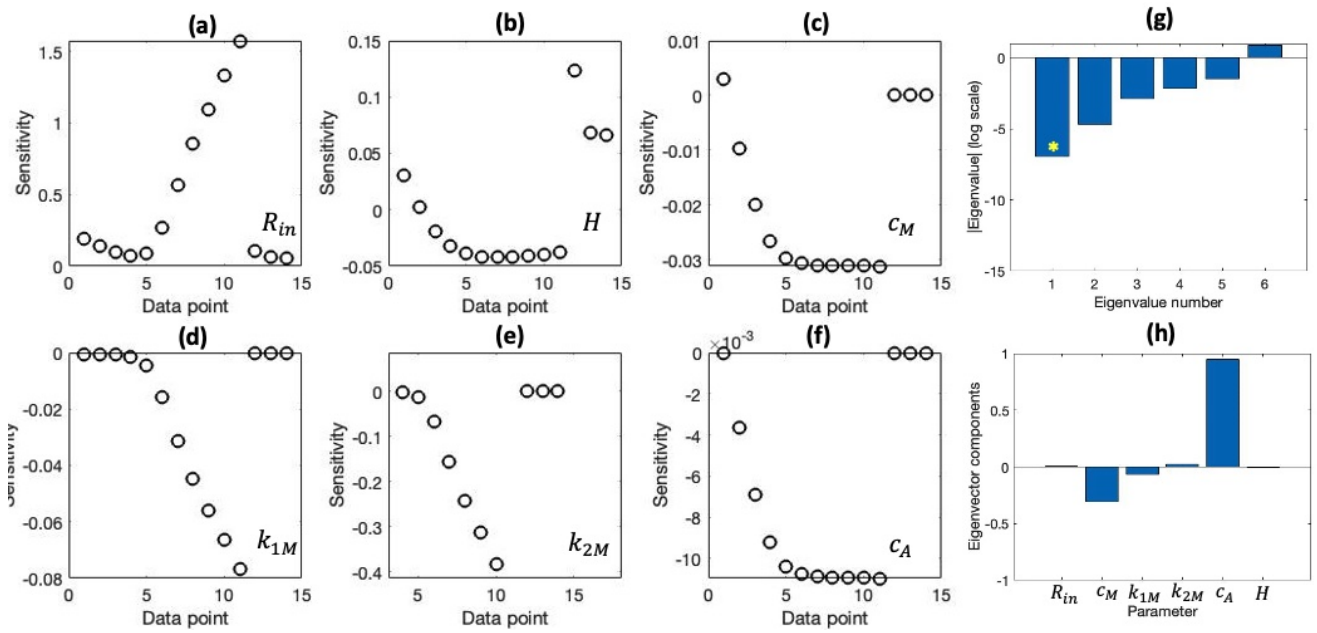

Figure 6 Identifiability results computed using eigendecomposition of the information matrix ($\chi^T\chi$) for the reduced 6 parameter model with data from the control (CTR) animals: (a-f) normalized parameter sensitivities for the 6 estimated parameters across the 14 data points; (g) log-plot of the eigenvalues of $\chi^T\chi$; (h) components of the eigenvector of $\chi^T\chi$ corresponding to the smallest eigenvalue of $\chi^T\chi$ ($\eta \approx 10^{-7}$) (asterisk).

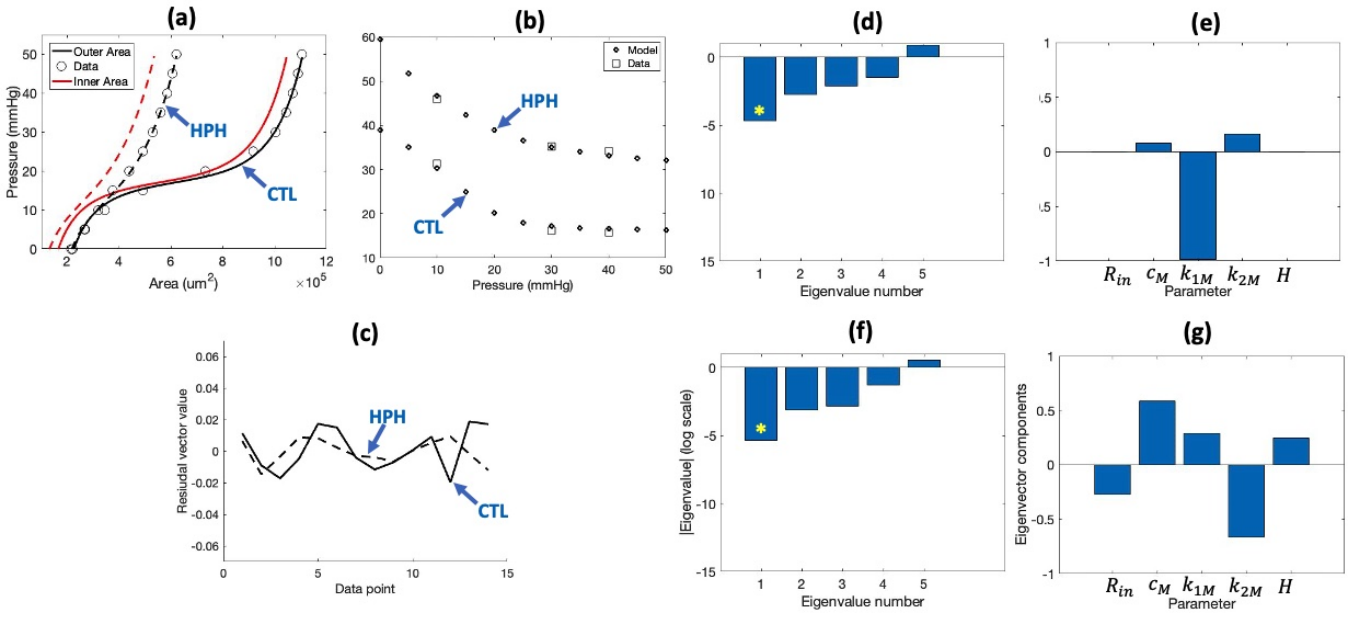

Figure 7 Parameter estimation and identifiability results for the reduced 5-parameter model for the control (CTL) and hypertensive animals, illustrated for case HPH^b: (a) pressure vs. area model predictions of the outer area (black) vs. data (circles) and the inner area (red); (b) wall thickness vs. pressure model predictions compared to the 3 data points (squares); (c) plot of the residual vector (13) across the 14 data points; (d,f) log-plot of the eigenvalues of $\chi^T\chi$ in the normotensive (d) and hypertensive (f) animals; (e,g) components of the eigenvector of $\chi^T\chi$ corresponding to the smallest eigenvalue of $\chi^T\chi$ (asterisk) in the control (e) and hypertensive (g) animals.

with collagen stiffness. Concurrently, in the hypertensive animals there is a substantial drop in the elastic modulus c_M (5.07kPa & 5.33kPa vs. 21.98kPa), associated with elastin, relative to the control animals. In the hypertensive case, 7 of 11 initial values of the wall thickness parameter (H) result in identical parameter estimates (Table 2), with the other 4 cases resulting in curve fits of poor quality.

For this reduced model, subset selection evaluating the eigenvalues and eigenvectors of $\chi^T\chi$ (Fig. 7d-g) for the estimated parameters (Table 2, Fig. 7d-g) reveals that identifiablity of the estimated parameters improves significantly (Fig. 7d,f). Nevertheless, it is instructive to examine the eigenvectors for the smallest eigenvalue (Fig. 7e,g). Based on the observations that k_{1M} is a dominant component in the control case (Fig. 7e) and that k_{1M} and c_M share the same units, we examine the possibility of a parameter dependency in the next section using our final 4-parameter reduced order model.

3.4 | Parameter dependencies in reduced-order model (4 parameters)

We study the implications of fixing one of these two parameters, for both the control and hypertensive animals. The final model fixes c_M while still estimating k_{1M}, i.e., analysis in this section estimates the 4 parameters,

$$\mathbf{q_4} = \left[R_{in}, H, k_{1M}, k_{2M}\right]. \tag{17}$$

The fixed parameter c_M is varied about its estimated value in the 5-parameter model. For brevity, in the hypertensive animals results are shown only for case HPH^b. Curve fits using this hypertensive model with an estimated value of H less than $1.05 \times 45.456\mu$m (Table 2, CTL, $m = 5$) are rejected to ensure (some) wall thickening. Since we do not have data from independent experiments for c_M, we repeat optimization while varying this parameter about its estimated value in the HPH^b model with $m = 5$ (Table 2, last column). To preserve quality of the curve fits, parameter ranges are determined by enforcing the cost increase to be no more than 10% (to two decimal places) relative to the values in Table 2, and across the range of initial values for H (see Table 4). Based on this criteria, the maximum cost used as a cutoff is set to $\mathcal{J} = 1.86 \cdot 10^{-4}$ (CTL) and $\mathcal{J} = 0.58 \cdot 10^{-4}$ (HPH^b).

The resulting estimated parameter ranges are reported in Table 3. The corresponding curve fits are not shown as they were visually identical to those shown in Fig. 7. For the hypertensive animals, the estimated value of k_{1M} varies directly with the (fixed) value of c_M and inversely with the estimated value of k_{2M}. For the control animals, the estimated value of k_{1M} varies inversely with both the (fixed) value of c_M and with the estimated value of k_{2M}, albeit over a smaller range of k_{2M} when compared to the hypertensive case. For the hypertensive animals, the geometric parameter ranges exhibit significant increases in both vessel wall inner radius R_{in} and reference wall thickness H. Furthermore, the ranges of values for the hypertensive elastic moduli associated with collagen (k_{1M}, k_{2M}) are substantially higher while the range of values for the modulus associated with elastin (c_M) is substantially lower, compared to the control animals.

4 | DISCUSSION

This study presents a novel data-driven approach yielding a reduced-order model predicting pressure-induced changes in lumen area and wall thickness by encoding a two-layer nonlinear hyperelastic HGO model incorporating residual stresses and anisotropy. This model is obtained by calibrating dynamics to pressure and wall thickness data from [28] for control and hypertensive mice. In the hypertensive animals, pulmonary hypertension is induced by placing the animals in a hyperbaric chamber exposing them to hypoxia for 10 days. Model calibration and systematic model reduction are achieved by combining sensitivity analysis, subset selection, parameter estimation and physical plausibility arguments. The results demonstrate that this detailed structural continuum mechanics model, containing a large number of parameters, can be systematically reduced to capture differences in key model parameters between control and hypertensive animals. We note that our full (initial) model, which contains several unidentifiable parameters, could be integrated into 1D cardiovascular network models by fixing these parameters at nominal values. For example, choices of such nominal values could be motivated by physiological hypotheses for mechanisms of remodeling due to disease; the identifiable parameters would still be estimated via optimization. Overall, the presence of several unidentifiable parameters can have adverse consequences when values calibrated on one type of biomechanical loading are used to simulate or predict responses under different loading conditions. This risk is much less when the model parameters retained, and estimated using data, are both identifiable and structurally meaningful, as is the outcome of the methodology presented in this study.

To our knowledge, this is the first study to carry out robust parameter estimation and local sensitivity based model reduction by simultaneously predicting the increase in lumen area and the decrease in wall thickness as pressure is increased in both

healthy and diseased animals. While prior studies (e.g. [37] in the mouse carotid artery) have demonstrated that HGO models can be overparameterized in the context of data, the analysis in [37] was carried out in an ad hoc or observational manner; by contrast our approach is systematic and more mathematically robust. A different study that applied the HGO model to healthy porcine pulmonary arteries assumed equal material properties in the media and adventitia *a priori* [38]. In another study, local sensitivity analysis methods were combined with optimization to investigate healthy myocardium [39], but systematic model reduction in the context of data comparing measurements from healthy and diseased samples was not considered.

Our results reveal that coupled biomechanical responses for both vessel lumen and vessel wall deformation can be accurately captured using a model that retains a single set of three elastic moduli delineating the contributions of collagen and elastin under the loading protocol of the associated experiments. Specifically, the material parameter associated with elastin (c_M) is the dominant contributor to nonlinear stiffening in the control animals. By contrast, in the hypertensive animals, the contribution of c_M is much less. Nonlinear stiffening is dominated by material parameters associated with collagen (k_{1M}, k_{2M}). Taken together, these findings are consistent with well-known increases in collagen content in the wall of large pulmonary arteries with hypoxia-induced PH [5, 6].

Our analysis considers two hypertensive cases (HPH^a and HPH^b). While one case (HPH^b) is based on the only known measurements of collagen fiber angles in a (right) pulmonary artery [34], we note that their hypoxic exposure was for a much longer and more variable duration (3-6 weeks) across the mice. Our data is from the LPA and based on a less variable hypoxic exposure of 10 days per mouse (§2.4). A comparative study in calves subjected to 14 days of hypoxic exposure found less evidence of remodeling in the RPA versus the LPA in the same animals [40]. Another study reported different remodeling rates in the RPA and the LPA, but based on a linear elastic response function within the quasilinear viscoelastic modeling framework [41]. Taken together, these studies potentially support the lack of evidence of hypoxia-induced RPA wall thickening in [34]. By contrast, our data and analysis demonstrate clear evidence of murine LPA wall thickening under 10 days of hypoxic exposure. A limitation of our model is the assumption of fixed collagen fiber angles, whereas future studies could extend the model to more realistically account for fiber dispersion in the vessel wall [42].

The robustness of our model and approach is evidenced by its accurate and simultaneous prediction of both pressure and wall thickness changes under deformation, for both control and hypertensive data sets. Our systematic approach to parameter identifiability, subset selection and model reduction decreased the overall number of parameters in the model while preserving the quality of curve-fits to the data at each stage of the iterative procedure. Overall, our methodological approach extracts information from the data that can be challenging to observe qualitatively. For example, in moving from the two-layer 8-parameter model to the two-layer 6-parameter model, parameter identifiability improved significantly. This improvement is evidenced by the large drop in the magnitude of the smallest eigenvalues (Fig. 4a vs. Fig. 6g). Hence, while our calibrated two-layer model could be used to formulate a pressure-area relation with a delineated media and adventitia, we contend that such a model is less well-calibrated due to the outstanding unidentifiable parameter (Fig. 6h). In particular, the robustness and accuracy of parameter estimates and ensuing simulations decreases as the number of parameters deemed to be unidentifiable (and thus fixed at nominal values) increases.

Limitations include common parameter estimation challenges when the number of model parameters and/or variables is greater than the number of variables for which data is available, as well as the lack of known nominal values for some model parameters in large pulmonary arteries. One challenge is non-uniqueness of parameter estimates due to the infeasability of guaranteeing a solution of the optimization problem that is a global minimum of the cost function across the parameter landscape. A second challenge is the local nature of sensitivity measures underlying the identifiability techniques used in this study, i.e., the final reduced model is not guaranteed to be unique. This can be a problem if translating the model to other diseases or vessels composed of the same tissues, but with different distribution of tissue components. The accuracy and robustness of the approaches presented in this study can be enhanced through both extended *ex vivo* and *in vivo* studies informed by the model presented here. Our approach for sensitivity and identifiability analysis and model reduction is rooted in prior works describing parameter subset selection techniques [29, 30, 43, 32] using an eigendecomposition of the matrix $\chi^T\chi$, but similar results could likely be obtained using other methods. While global sensitivity analysis techniques exist [44, 45, 46], most subset selection techniques are local. The method for identifiability analysis used here is based on eigenvalues but, as discussed in several previous studies, similar results can be obtained using other methods [47, 31, 48]. Overall, sensitivities or unidentifiable parameters for particular variables or quantities of interest can suggest which types of data will be most influential in an expanded data set. Where practical, examples of extensions include augmentation of *ex vivo* biomechanical testing to include measurement of the vessel opening angle, as well as incorporation of *in vivo* data measuring BP, flow and lumen area prior to sacrifice

of the animal(s). Our model is also based on assumptions of hyperelastic deformation and geometric idealization of the stress-free reference state (Fig. 1b) as a segment of a cylindrical ring; in reality, the vessel wall may exhibit viscoelastic effects under pressurization and/or deviate from circular arcs in the cut open rings.

5 | CONCLUSIONS

This study develops a data-driven reduced-order nonlinear elastic structural wall model for a healthy and hypertensive murine left pulmonary artery. Our methodology provides a systematic reduction of the two layer formulation to a single layer model that accurately fits data for both pressure-area dynamics and wall thickness changes, as functions of pressure. Our findings demonstrate that elastin parameters dominate nonlinear stiffening in the control animals while collagen parameters are much more influential in the hypertensive animals. The reduced order pressure-area relation developed in this study has the potential for incorporation into 1D cardiovascular network models of coupled fluid-solid dynamics in large pulmonary arteries. Some possible approaches include direct incorporation and coupling of the pressure-area relation within the 1D fluids network solver or, alternatively, using the pressure-area relation as a high fidelity model for emulation using simpler empirical models [20, 13, 22] or statistical models. Overall, the techniques and findings presented here demonstrate the potential for development and systematic reduction of more realistic models of key relations (e.g. pressure-area) through the integration of data-driven mathematical approaches for *ex vivo* experiments with modeling approaches predicting *in vivo* dynamics in cardiovascular biomechanics.

References

[1] McLaughlin VV, Archer SL, Badesch DB, et al. ACCF/AHA 2009 expert consensus document on pulmonary hypertension: A report of the American College of Cardiology Foundation task force on expert consensus documents and the American Heart Association. *Circulation*. 2009; 119:2250-2294.

[2] Simonneau G, Montani D, Celermajer DS, et al. Haemodynamic definitions and updated clinical classification of pulmonary hypertension. *Eur Respir J*. 2019; 53:1801913.

[3] Michiels C. Physiological and pathological responses to hypoxia. *Am J Pathol*. 2004; 164:1875-1882.

[4] Rich S, Rabinovitch M. Diagnosis and treatment of secondary (non-category 1) pulmonary hypertension. *Circulation*. 2008; 118:2190-2199.

[5] Ooi CY, Wang Z, Tabima DM, Eickhoff JC, Chesler NC. The role of collagen in extralobar pulmonary artery stiffening in response to hypoxia-induced pulmonary hypertension. *Am J Physiol*. 2010; 299:H1823–1831.

[6] Wang Z, Chesler NC. Role of collagen content and cross-linking in large pulmonary arterial stiffening after chronic hypoxia. *Biomech Model Mechanobiol*. 2012; 11:279–289.

[7] Wohrley JD, Frid MG, Moiseeva EP, et al. Hypoxia selectively induces proliferation in a specific subpopulation of smooth muscle cells in the bovine neonatal pulmonary arterial media. *J Clin Invest*. 1995; 96:273-281.

[8] Stenmark KR, Fagan KA, Frid MG. Hypoxia-Induced pulmonary vascular remodeling: Cellular and molecular mechanisms, *Circ Res*. 2006; 99:675-691.

[9] Azer K, Peskin CS. A one-dimensional model of blood flow in arteries with friction and convection based on the Womersley velocity profile. *Cardiovasc Eng*. 2007; 7:51-73.

[10] Battista C, Bia D, German YZ, Armentano RL, Haider MA, Olufsen MS. Wave propagation in a 1D fluid dynamics model using pressure-area measurements from ovine arteries. *J Mech Med Biol*. 2016; 16:1650007.

[11] Chen WW, Gao H, Luo XY, Hill NA. Study of cardiovascular function using a coupled left ventricle and systemic circulation model. *J Biomech*. 2016; 49:2445-2454.

[12] Matthys KS, Alastruey J, Peiró J, et al. Pulse wave propagation in a model human arterial network: assessment of 1-D numerical simulations against in vitro measurements. *J Biomech*. 2007; 40:3476-86.

[13] Olufsen MS. Structured tree outflow condition for blood flow in larger systemic arteries. *Am J Physiol*. 1999; 276:H257–H268.

[14] Van de Vosse FN, Stergiopulos N. Pulse wave propagation in the arterial tree, *Ann Rev Fluid Mech*. 2011; 43:467-499.

[15] Colebank MJ, Qureshi MU, Rajagopal S, Krasuski RA, Olufsen MS. A multiscale model of vascular function in chronic thromboembolic pulmonary hypertension. *Am J Physiol*. 2021; 321:H318-H338

[16] Paun LM, Colebank MJ, Olufsen MS, Hill NA, Husmeier D. Assessing model mismatch and model selection in a Bayesian uncertainty quantification analysis of a fluid-dynamics model of pulmonary blood circulation. *J R Soc Interface*. 2020; 17:20200886.

[17] Qureshi MU, Vaughan GD, Sainsbury C, et al. Numerical simulation of blood flow and pressure drop in the pulmonary arterial and venous circulation. *Biomech Model Mechanobiol*. 2014; 13:1137-54.

[18] Colebank MJ, Qureshi MU, Olufsen, MS. Sensitivity analysis and uncertainty quantification of 1D models of pulmonary hemodynamics in mice under control and hypertesnive conditions. *Numer Meth Biomed Eng*. 2019; 37(11):e3242.

[19] Zhang H, Fujiwara N, Kobayashi M, et al. Development of patient-specific 1D-0D simulation based on MRI and SPECT data. *J Biorheol*. 2018; 32(1):2-8.

[20] Langewouters GJ, Wesseling KH, Goedhard WJ. The static elastic properties of 45 human thoracic and 20 abdominal aortas in vitro and the parameters of a new model. *J Biomech*. 1984; 17:425-35.

[21] Qureshi MU, Colebank MJ, Paun LM, et al. Hemodynamic assessment of pulmonary hypertension in mice: a model based analysis of the disease mechanism. *Biomech Model Mechanobiol*. 2018; 18:219-243.

[22] Valdez-Jasso D, Bia D, Zócalo Y, Armentano RL, Haider MA, Olufsen MS. Linear and nonlinear viscoelastic modeling of aorta and carotid pressure-area dynamics under in vivo and ex vivo conditions. *Ann Biomed Eng*. 2011; 39:1438-1456.

[23] Holzapfel GA, Gasser TC, Ogden RW. A new constitutive framework for arterial wall mechanics and a comparative study of material models. *J Elasticity*. 2000; 61:1-48.

[24] Ramachandra AB, Humphrey JD. Biomechanical characterization of murine pulmonary arteries. *J Biomech*. 2019; 84:18-26.

[25] Zambrano BA, McLean NA, Zhao X, et al. Image-based computational assessment of vascular wall mechanics and hemodynamics in pulmonary arterial hypertension patients. *J Biomech*. 2018; 68:84-92.

[26] Huang W, Sher YP, Delgado-West D, Wu JT, Peck K, Fung YC. Tissue remodeling of rat pulmonary artery in hypoxic breathing. I. Changes of morphology, zero-stress state, and gene expression. *Ann Biomed Eng*. 2001; 29:535-551.

[27] Xu M, Platoshyn O, Makino A, et al. Characterization of agonist-induced vasoconstriction in mouse pulmonary artery. *Am J Physiol*. 2008; 294: H220-H228.

[28] Tabima DM, Chesler NC. The effects of vasoactivity and hypoxic pulmonary hypertension on extalobar pulmonary arterial biomechanics. *J Biomech*. 2010; 43:1864-1869.

[29] Burth M, Verghese GC, Vélez-Reyes M. Subset selection for improved parameter estimates in on-line identification of a synchronous generator. *IEEE Trans Power Syst.* 1999; 14:218-225.

[30] Cintrón-Arias A, Banks HT, Capaldi A, Lloyd AL. A sensitivity matrix based methodology for inverse problem formulation. *J Inverse Ill-posed*. 2009; 17:545-564.

[31] Miao H, Xia X, Perelson AS, Wu H. On identifiability of nonlinear ODE models and applications in viral dynamics. *SIAM Rev*. 2011; 53:3-39.

[32] Quaiser T, Mönnigmann M. System identifiability testing for unambiguous mechanistic modeling – application to JAK-STAT, MAP kinase, and NF-κ B signaling pathway models. *BMC Systems Biology*. 2009; 3:50.

[33] Shampine LF. Vectorized adaptive quadrature in MATLAB. *J Comp Appl Math*. 2008; 211:131-140.

[34] Manning EP, Ramachandra AB, Schupp JC, et al. Mechanisms of hypoxia-induced pulmonary arterial stiffening in mice revealed by a functional genetics assay of structural, functional, and transcriptomic data. *Front Physiol*. 2021; 12:726253.

[35] Nelder J, Mead R. A simplex method for function minimization. *Comput J*. 1965; 7:308-313.

[36] Rothenberg TJ. Identification in parametric models. *Econometrica*. 1971; 39:577-591.

[37] Badel P, Avril S, Lessner S, Sutton M. Mechanical identification of layer-specific properties of mouse carotid arteries using 3D-DIC and a hyperelastic anisotropic constitutive model. *Comput Methods Biomech Biomed Engin*. 2012; 15(1):37-48.

[38] Pillalamarri NR, Patnaik SS, Piskin S, Gueldner P, Finol EA. Ex vivo regional mechanical characterization of porcine pulmonary arteries. *Exp Mech*. 2021; 61:285-303.

[39] Gao H, Li WG, Cai L, Berry C, Luo XY. Parameter estimation in a Holzapfel–Ogden law for healthy myocardium. *J Eng Math*. 2015; 95:231-248.

[40] Lammers SR, Kao PH, Jerry Qi H, et al. Changes in the structure-function relationship of elastin and its impact on the proximal arterial mechanics of hypertensive calves. *Am J Physiol Heart Circ Physiol*. 2008; 295(4):H1451-H1459.

[41] Pursell ER, Velez-Rendon D, Valdez-Jasso D. Biaxial properties of the left and right pulmonary arteries in a monocrotaline rat animal model of pulmonary arterial hypertension. *J Biomech Engng*. 2016; 138:111004-1.

[42] Holzapfel GA, Ogden RW, Sherifova S. On fibre dispersion modelling of soft biological tissues: a review. *Proc Math Phys Eng Sci*. 2019; 475:1-22.

[43] Pearce KJ, Nellenbach K, Smith RC, Brown AC, Haider MA. Modeling and parameter subset selection for fibrin polymerization kinetics with applications to wound healing. *Bull Math Biol*. 2021; 83:47.

[44] Kucherenko S, Iooss B. Derivative-based global sensitivity measures. In: Ghanem R, Higdon D, Owhadi H. eds. *Handbook of Uncertainty Quantification*. New York, NY; Springer; 2017:1241-1263

[45] Marquis AD, Arnold A, Dean-Bernhoft C, Carlson BE, Olufsen MS. Practical identifiability and uncertainty quantification of a pulsatile cardiovascular model. *Math Biosci*. 2018; 304:9-24.

[46] Saltelli A, Ratto M, Andres T, et al. *Global sensitivity analysis: the primer*. Chichester, UK: John Wiley and Sons; 2008.

[47] Haargaard Olsen C, Ottesen JT, Smith RC, Olufsen MS. Parameter subset selection techniques for problems in mathematical biology. *Biol Cybern*. 2019; 113:121-138.

[48] Olufsen MS, Ottesen JT. A practical approach to parameter estimation applied to model predicting heart rate regulation. *J Math Biol*. 2013; 67:39-68.

6 | LIST OF FIGURE CAPTIONS

Figure 1 - Foundations of the nonlinear hyperelastic wall model: (a) Illustration of a cross-section of a large artery wall (redrawn from [23]); (b) the stress-free reference state Ω_0 defined in equation (1) where R_{in} is the inner radius, R_{out} is the outer radius, H is the wall thickness, L is the axial length and α is the opening angle; (c) the current configuration Ω defined in (2). Note that the (deformed) inner radius (r_{in}), outer radius (r_{out}) and axial length (l) are all determined after the model equations are solved.

Figure 2 - Results from estimating 8 parameters (listed in Table 1) for the control (CTL) animals. (a) pressure vs. area, model predictions of the outer area (black) vs. data (circles) and the inner area (red); (b) wall thickness vs. pressure model predictions

compared to the 3 data points (squares); (c) the residual vector (13) across the 14 data points.

Figure 3 - Normalized parameter sensitivities for the control (CTL) animals with 8 estimated parameters across the 14 data points.

Figure 4 - Identifiability results using the eigendecomposition of the information matrix ($\chi^T\chi$) for the control (CTL) animals with 8 estimated parameters: (a) log-plot of the eigenvalues of $\chi^T\chi$; (b) components of the eigenvector of $\chi^T\chi$ corresponding to the smallest eigenvalue of $\chi^T\chi$ ($\eta \approx 10^{-14}$) (asterisk).

Figure 5 - Parameter estimation results for the reduced model for the control (CTL) animals with 6 estimated parameters: (a) pressure vs. area model predictions of the outer area (black) vs. data (circles) and the inner area (red); (b) wall thickness vs. pressure model predictions compared to the 3 data points (squares); (c) plot of the residual vector (13) across the 14 data points.

Figure 6 - Identifiability results computed using eigendecomposition of the information matrix ($\chi^T\chi$) for the reduced 6 parameter model with data from the control (CTR) animals: (a-f) normalized parameter sensitivities for the 6 estimated parameters across the 14 data points; (g) log-plot of the eigenvalues of $\chi^T\chi$; (h) components of the eigenvector of $\chi^T\chi$ corresponding to the smallest eigenvalue of $\chi^T\chi$ ($\eta \approx 10^{-7}$) (asterisk).

Figure 7 = Parameter estimation and identifiability results for the reduced 5-parameter model for the control (CTL) and hypertensive animals, illustrated for case HPH^b: (a) pressure vs. area model predictions of the outer area (black) vs. data (circles) and the inner area (red); (b) wall thickness vs. pressure model predictions compared to the 3 data points (squares); (c) plot of the residual vector (13) across the 14 data points; (d,f) log-plot of the eigenvalues of $\chi^T\chi$ in the normotensive (d) and hypertensive (f) animals; (e,g) components of the eigenvector of $\chi^T\chi$ corresponding to the smallest eigenvalue of $\chi^T\chi$ (asterisk) in the control (e) and hypertensive (g) animals.

7 | TABLES

Table 1 Estimated parameter values for the control (CTL) animals with the 8-parameter model (column 5) and the reduced 6-parameter model (column 6).

	Param.	Units	Initial	Baseline (§3.1)	Reduced (§3.2)
m				8	6
Geom.	R_{in}	μm	1000	376.711	376.666
	H	μm	$T_1^{data} \cdot [1, 1+\gamma]$	45.428	45.430
			($\gamma = [1.0, 1.5]$)	($\gamma = 0.1$)	($\gamma = 0.4$)
Media	c_M	kPa	10	24.835	25.057
	k_{1M}	kPa	1	0.271	0.299
	k_{2M}	-	0.839	2.064	2.083
Adv.	c_A	kPa	10	16.460	15.990
	k_{1A}	kPa	0.3	0.035	0.000 (fixed)
	k_{2A}	-	0.711	2.734	0.000 (fixed)
$\mathcal{J}$ ($\cdot 10^{-4}$)		-		1.7306	1.7324

Table 2 Estimated parameter values for the reduced 5-parameter model for control (CTL) (column 6) and hypertensive (HPH) (column 5) animals. For comparison, results for the reduced 6-parameter model are also shown (column 4).

	Param.	Units	Initial	CTL (§3.2)	CTL (§3.3)	HPH[a] (§3.3)	HPH[b] (§3.3)
m				6	5	5	5
Geom.	R_{in}	μm	1000	376.666	377.378	513.688	497.959
	H	μm	$T_1^{data} \cdot [1, 1+\gamma]$	45.430	45.356	48.557	49.953
			($\gamma = [0.0, 0.5]$)	($\gamma = 0.4$)	($\gamma = [0.0, 0.5]$)	($\gamma = [0.0, 0.3]$)	($\gamma = [0.0, 0.3]$)
Media	c_M	kPa	10	25.057	21.984	5.073	5.327
	k_{1M}	kPa	1	0.299	0.185	3.060	1.899
	k_{2M}	-	0.839	2.083	2.188	7.082	7.119
Adv.	c_A	kPa	10	15.990	$= c_M$	$= c_M$	$= c_M$
	k_{1A}	kPa		(fixed at 0.0)	$= k_{1M}$	$= k_{1M}$	$= k_{1M}$
	k_{2A}	-		(fixed at 0.0)	$= k_{2M}$	$= k_{2M}$	$= k_{2M}$
$\mathcal{J}$ ($\cdot 10^{-4}$)		-		1.7324	1.6931	0.5297	0.5298

Table 3 Estimated parameter ranges for the final model in both the control (CTL) and hypertensive (HPH[b]) animals based on optimization with 4 parameters. The cost $\mathcal{J}$ was allowed to increase by no more than 10% in establishing the estimated parameter ranges.

	Param.	Units	Initial	CTL (§3.4)	HPH[b] (§3.4)
m				4	4
Geom.	R_{in}	μm	1000	374.46-380.45	426.50-522.97
	H	μm	$T_1^{data} \cdot [1, 1+\gamma]$	44.73-45.91	47.77-57.35
			($\gamma = [0.0, 0.5]$)	($\gamma = [0.0, 0.5]$)	($\gamma = [0.0, 0.3]$)
Media	c_M	kPa		20.12-23.85 (fixed)	4.79-7.62 (fixed)
	k_{1M}	kPa	1	0.11-0.31	1.77-1.84
	k_{2M}	-	0.839	1.96-2.43	5.01-8.03
Adv.	c_A	kPa		$= c_M$	$= c_M$
	k_{1A}	kPa		$= k_{1M}$	$= k_{1M}$
	k_{2A}	-		$= k_{2M}$	$= k_{2M}$
$\mathcal{J}$ ($\cdot 10^{-4}$)		-		1.69-1.86	0.53-0.58

8 | APPENDIX

8.1 | Complete set of model parameters

For convenience, the full set of model parameters, their descriptions, units, designation of parameter type (estimated, fixed, dependent or eliminated) and the associated fixed or initial values are summarized in Table 4.

□

Table 4 List of all parameters for the model developed in this study. Each parameter is denoted as estimated (E), fixed (F), dependent (D) or eliminated (El.). When different values are used for the hypertensive case, values are denoted as c (normotensive), h^a for the HPH-A model and h^b for the HPH-B model. Estimated parameters listed with an asterisk (*) are ultimately fixed (during the course of the model reduction). Note that the model no longer depends on the parameter L when the twist angle Φ is assumed to be zero (see (3)).

Type	Param.	Description	Units	Role	Fixed Value	Initial Value
Geom.	R_{in}	Inner radius in Ω_0	μm	E		1000 [28]
	R_{out}	Outer radius in Ω_0	μm	D	$R_{in} + H$	N/A
	H	Vessel wall thickness in Ω_0	μm	E		$[1, 1.5] \cdot T_1^{data}$[28]
	H_M	Media thickness in Ω_0	μm	F	0.63H/0.63H/0.60H (c/h^a/h^b) [34]	N/A
	α	Opening angle in Ω_0	deg.	F	94.2 [27](c),[26](h^a,h^b)	
	L	Axial length in Ω_0	μm	El.	N/A	
	λ_z	Axial stretch in deformation	-	F	1.4 [28]	
	Φ	Twist angle in deformation	-	F	0.0	
Med.	c_M	elastic modulus (iso.)	kPa	E		10
	k_{1M}	elastic modulus (aniso.)	kPa	E		1
	k_{2M}	elastic parameter (aniso.)	-	E		0.839 [23]
	β_M	collagen fiber angle	deg.	F	54.45/54.45/56.58 (c/h^a/h^b) [34]	
Adv.	c_A	elastic modulus (iso.)	kPa	E*		10
	k_{1A}	elastic modulus (aniso.)	kPa	E*		0.3
	k_{2A}	elastic parameter (aniso.)	-	E*		0.711 [23]
	β_A	collagen fiber angle	deg.	F	54.45/54.45/56.58 (c/h^a/h^b) [34]	